Synthesis and aggregation behavior of biohybrid amphiphiles composed of a tripeptidic head group and a polystyrene tail†

A. (Ton) J. Dirks, Sander S. van Berkel, Helene I. V. Amatdjais-Groenen, Floris P. J. T. Rutjes, Jeroen J. L. M. Cornelissen* and Roeland J. M. Nolte

Received 23rd September 2008, Accepted 26th January 2009
First published as an Advance Article on the web 4th March 2009
DOI: 10.1039/b816615c

The modular synthesis and self-assembly behavior of a set of peptide-polymer hybrid amphiphiles is described. Gly-Gly-Arg derivatives were conjugated to one of the ends of hetero-telechelic polystyrene (PS) *via* either the Cu-catalyzed azide-alkyne 1,3-dipolar cycloaddition (CuAAC) reaction or conventional peptide coupling chemistry. Both conjugation strategies proved to be efficient and they were also applied sequentially to create a biohybrid ABA-type triblock copolymer, which can be considered as a macromolecular bolaamphiphile. In the synthesis of the regularly-shaped peptide-PS amphiphiles (*i.e.* AB-type) two polymer lengths ($n = 21$ and $n = 49$) were employed having additional variations in their end group composition. As expected, the structural variations were demonstrated not to influence the self-assembly behavior of the biohybrids in water, and comparable vesicles were formed in all cases. At the air/water interface, the structural variations had a greater impact on the self-assembly of the biohybrids, especially for the phase transition from *gas* to *liquid* because it is dominated by steric interactions between the polymer chains. In a condensed phase (which closely resembles the situation in a bilayer vesicle), the packing of various biohybrids was found to be comparable. The interfacial self-assembly behavior of the bolaamphiphile ($n = 21$) was also studied and this compound probably formed multi-layered structures on the water surface. In aqueous solution the bolaamphiphile formed spherical aggregates similar to the regular peptide-PS amphiphiles. Although these assemblies appeared to be vesicular, their exact nature remains unclear.

Introduction

Biohybrid amphiphiles derived from sequence-defined peptides are powerful building blocks for the construction of functional self-assembled materials.[1-3] A common approach to prepare such hybrid amphiphiles is to equip the *N*- or *C*-terminus of a peptide with one or more long alkyl chains.[2] In this way, several peptides have been modified and the resulting amphiphiles frequently self-assembled into functional nanofibers.[4-8] Extending the hydrophobic alkyl chain to a well-defined polymer has also been shown to create effective self-assembling biohybrids.[9-13] These peptide-based block copolymers are of particular interest because macromolecular amphiphiles generally form more stable aggregates than their low molecular weight counterparts.

In order to prepare biohybrid block copolymers with a sequence-defined peptide segment, several routes have been developed.[14-16] Essentially, these routes follow two general approaches: (i) the coupling of a preformed polymer to a peptide (*i.e.* grafting-to), and (ii) the propagation (growing) of a polymer from a peptide initiator (*i.e.* grafting-from). The latter approach has recently received a lot of attention and has been employed with various peptide initiators in polymerizations from a solid support[10,17,18] and in solution.[9,19-28] For example, Wooley *et al.*[10] have used a resin-bound antimicrobial peptide to prepare functional initiators for nitroxide-mediated polymerization (NMP)[29] and atom transfer radical polymerization (ATRP).[30,31] Sequential polymerization of *tert*-butyl acrylate and styrene from these initiators gave rise to well-defined ABC-type triblock copolymers.[10] After cleavage from the resin and hydrolysis of the *tert*-butyl esters, the biohybrids formed micellar aggregates in water and displayed an enhanced antimicrobial activity compared to the native peptide. In another example with respect to amphiphilic peptide-polymer hybrids, van Hest and coworkers employed the grafting-from approach to prepare ABA-type triblock copolymers with Ac-Ser-Ala-Gly-Ala-Gly-Glu-Gly-Ala-Gly-Ala-Gly-Ser-Gly-OH (a β-hairpin forming peptide) as the inner block.[9] To this end, both serine residues of the peptide were functionalized with α-bromo esters, and methyl methacrylate (MMA) was polymerized in two directions using ATRP. Suspension of the triblock copolymer in a THF-water mixture followed by the removal of THF resulted in the formation of vesicles and large compound micelles (LCMs).

Building up a polymer from a peptide initiator is an elegant way to prepare peptide-polymer conjugates. However, for the synthesis of amphiphilic biohybrids it may often be more convenient to follow the grafting-to approach, because this allows the contrasting blocks to be prepared separately under optimal conditions, which are likely to diverge for each block. In this way, furthermore, all segments can be fully characterized

Institute for Molecules and Materials, Radboud University Nijmegen, Toernooiveld 1, 6525 ED Nijmegen, Netherlands. E-mail: J.Cornelissen@science.ru.nl; Fax: (+31) 24 365 2929; Tel: (+31) 24 365 2381

† Electronic supplementary information (ESI) available: Experimental procedures for the preparation of peptides **5** and **6** and self-assembly of **9b** at elevated temperature. See DOI: 10.1039/b816615c

without encountering the complications caused by an amphiphilic character, *e.g.* solubility issues. A prerequisite of the grafting-to approach, obviously, is an efficient coupling strategy to link together bulky building blocks. Among the various reactions that can be considered for this purpose, the Cu(I)-catalyzed azide-alkyne 1,3-dipolar cycloaddition (CuAAC) reaction has recently proven to be of particular value.[32-38] We and others have demonstrated that peptide-polymer hybrids can be readily prepared by employing the CuAAC in a modular approach.[11,39,40] In our previous synthetic studies we selected for the peptide part an alkyne-functionalized Gly-Gly-Arg derivative tagged with fluorescent 7-amino-4-methyl coumarin (AMC), such that the material could easily be tracked during work-up and characterization. Azide-terminated polystyrene (PS) was used as the complementary block and was synthesized by ATRP of styrene followed by the displacement of the bromide end group with Me_3SiN_3 and tetrabutylammonium fluoride (TBAF). With the aid of CuBr/*N*,*N*,*N*′,*N*″,*N*‴-pentamethyldiethylenetriamine (PMDETA) as a catalyst, the two building blocks were efficiently coupled together to yield a peptide-polymer amphiphile that formed vesicles in aqueous environment.

As peptide-polymer amphiphiles are a promising class of compounds for the construction of bioactive nano-sized structures, it is of interest to investigate the synthesis and aggregation behavior of these compounds. Therefore, we decided to further explore our modular synthetic approach for the preparation of PS-GlyGlyArg-AMC hybrids. We were interested in comparing the CuAAC to standard peptide coupling chemistry, which has also proven to be useful for the preparation of peptide-polymer hybrids.[12] For this comparative study, a PS chain was synthesized in such a way that the α-terminus could readily be transformed into a carboxylic acid, while at the ω-end an azide moiety could be installed. Hence, the same precursor polymer can be tailored for both coupling techniques, employing either alkyne-functionalized Gly-Gly-Arg-AMC or the native peptide as the complementary part. Moreover, we envisioned that starting from a polymer with both an azide and a carboxylic acid end group should allow sequential coupling of two peptide segments, to create a biohybrid ABA-type triblock copolymer which can be considered as a macromolecular bolaamphiphile. Bolaamphiphiles are an interesting class of amphiphiles that have been used to create monolayer membrane (MLM) vesicles, but they are also capable of forming a variety of other assemblies.[41]

In this article, we discuss the modular synthesis of peptide-PS hybrid amphiphiles by making use of the CuAAC reaction or peptide coupling chemistry. Furthermore, the synthesis of a biohybrid bolaamphiphile is described by combination of the two coupling techniques. Throughout exploration of the synthetic methods, a series of biohybrid amphiphiles was obtained and the aggregation behavior of these compounds is reported both in solution and at the air/water interface.

Experimental

Materials

All chemicals were obtained from commercial sources and used without further purification, unless otherwise stated. Analytical thin layer chromatography (TLC) was performed on Merck precoated silica gel 60 F-254 plates (layer thickness 0.25 mm) with the indicated eluent and visualization by ultraviolet (UV) irradiation at $\lambda = 254$ nm and/or $\lambda = 366$ nm. Preparative thin layer chromatography (Prep-TLC) was performed on Merck precoated silica gel 60 F-254 plates (layer thickness 1.00 mm) with concentration zone and visualization by UV irradiation at $\lambda = 254$ nm and/or $\lambda = 366$ nm. Purification by silica gel chromatography was carried out using Acros (0.035-0.070 mm, pore diameter *ca.* 6 nm) silica gel. The water used for the self-assembly studies was deionised using a Labconco Water Pro PS purification system. Styrene was distilled under reduced pressure prior to use. THF was distilled under nitrogen from sodium/benzophenone. CH_2Cl_2 was distilled under nitrogen from CaH_2. Anhydrous DMF was obtained from Biosolve. Dialysis tubing (regenerated cellulose membrane) with a molecular weight cut-off (MWCO) of 3 kDa was obtained from Spectra/Por.

General analytical techniques

NMR spectra were recorded on Bruker DMX 300 (300 MHz) and Varian Inova 400 (400 MHz) spectrometers. ^{1}H NMR chemical shifts (δ) are reported in parts per million (ppm) relative to a residual proton peak of the solvent; $\delta = 7.26$ for $CDCl_3$. Multiplicities are reported as: s (singlet), d (doublet), t (triplet), q (quartet), dd (doublet of doublets), or m (multiplet). Broad peaks are indicated by the addition of br. Infrared (IR) spectra were recorded on an ATI Matson Genesis Series FTIR spectrometer fitted with an ATR cell. The vibrations (ν) are given in cm^{-1}. GC analysis was conducted on a Hewlett/Packard 5890 Series II gas chromatograph, equipped with a capillary column (HP1707, 25 m × 0.32 m × 0.25 μm), using flame/ionisation detection. Molecular weight distributions were measured with a Shimadzu SEC, equipped with a guard column and a PL gel 5 μm mixed D column (Polymer Laboratories) with differential refractive index (RI) and UV ($\lambda = 254$ nm and $\lambda = 330$ nm) detection using THF (1 mL min^{-1} at 35 °C) or NMP (1 mL min^{-1} at 65 °C) as an eluent. Polystyrene (PS) standards in the range of 580 to 377,400 Da were used for calibration. Matrix assisted laser desorption/ionisation time-of-flight (MALDI-ToF) mass spectra were measured on a Bruker Biflex III spectrometer. Indolecrylic acid (IAA) was used as a matrix. Samples were prepared by mixing 45 μL of a 20 mg mL^{-1} matrix solution in THF with 5 μL of a 2 mg mL^{-1} solution of polymer in THF. From this mixture 1 μL was spotted on the target plate.

Self-assembly in water

Two procedures were employed to induce self-assembly of biohybrids **7-10**; (i) 100 μL of amphiphile dissolved in THF (1 mg mL^{-1}) was injected into 1 mL of water *via* a syringe (at rt or 50 °C); (ii) water was added dropwise to a 0.15 mg mL^{-1} solution of amphiphile in THF (typically 1.8 mL) until the water content reached 40% (v/v). Subsequently, the mixture was dialyzed against water (500 mL) using a MWCO of 3 kDa. After 3 h of gentle stirring the medium was refreshed (2×). For both methods the final concentration of amphiphiles was *ca.* 0.09 mg mL^{-1}. The solutions were diluted once for TEM studies and ten times for dynamic light scattering measurements. Self-assembly of biohybrid **11** was achieved by dialysis from a DMF solution, following the same method as described above (ii). This sample was diluted ten times with water for further studies.

Transmission electron microscopy (TEM)

TEM images were obtained using a JEOL JEM 1010 microscope (60 kV) equipped with a charge-coupled device (CCD) camera. For peptide-PS conjugates **7-10**, samples were prepared by placing a carbon-coated copper grid on top of a droplet of aggregate suspension (either prepared *via* injection or dialysis). After 1 min the excess of water was drained off using filter paper. The grids were subsequently dried in air for 30 min followed by 1 h in high vacuum. The structures were visualised using platinum shadowing (with an Edwards model 306 coater) at an angle of approximately 45°. For compound **11** the aggregate suspension was placed on top of a carbon-coated copper grid and after 5 min half of the water volume was drained off with filter paper. The sample was further dried in air for approximately 3 h and high vacuum for 1 h before Pt shadowing was applied.

Cryo-scanning electron microscopy (cryo-SEM)

Cryo-SEM was performed on a JEOL JSM T300 microscope operating at 30 kV. The sample solution was quenched in nitrogen slush. Afterwards, the sample was freeze-fractured with standard procedures and transferred into the instrument. The sample was sublimed for 5 min before being inserted into the sample chamber.

Dynamic light scattering (DLS)

DLS experiments were carried out using a home-built setup fitted with a Coherent CR599 dye laser operating at 600 nm. Samples were loaded into a spherical glass cuvette which was placed in a water bath at 25 °C. Measurements were performed at angles of 30° and 60°. The average hydrodynamic radius of the particles was determined by CONTIN analysis.

Monolayer experiments

Pressure-Area (Π-A) isotherms were measured with a KSV minithrough Langmuir-Blodgett device with a water reservoir at 22 °C (RM6 Lauda). Monolayers were spread on the air-water interface from a $CHCl_3$ solution of biohybrids **7-10** (typically 50 μL of 1 mg mL^{-1}). Conjugate **11** was spread from a solution in 5% MeOH-$CHCl_3$ (50 μL of 1 mg mL^{-1}) or from a dilute solution in 1,2-dichloroethane (DCE) (200 μL of 0.2 mg mL^{-1}). In the latter case treatment with ultrasound (20 min at 40 °C) was applied to achieve complete dissolution. After incubation for 10 min the monolayers were compressed/decompressed at 10 cm^2 min^{-1}. Films were transported to carbon-coated copper grids, for TEM analysis, by horizontally lifting them from the surface.

α-*tert*-Butylcarboxy ω-bromo polystyrene (1)

Typical procedure (**1b**): Cu(I)Br (129.4 mg, 0.902 mmol) was placed in a Schlenk tube fitted with a stopper. The tube was evacuated and back-filled with argon (3×). After the evacuating cycles the stopper was replaced by a septum. An argon-purged mixture of anisole (0.5 mL, as internal standard for conversion analysis), *N*,*N*,*N*′,*N*″,*N*‴-pentamethyldiethylenetriamine (PMDETA, 214 μL, 0.903 mmol) and styrene (5.00 mL, 43.7 mmol) was added and the reaction vial was placed in a statically controlled oil bath at 90 °C. Subsequently, *tert*-butyl-2-bromo-isobutyrate (170 μL, 0.912 mmol) was added to the reaction mixture. Samples were taken periodically for conversion analysis by gas chromatography. The polymerization was stopped at 67% of conversion by cooling and exposing the catalyst to air. The reaction mixture was diluted with CH_2Cl_2 and washed with an aqueous ethylenediaminetetraacetic acid (EDTA) solution (0.065 M) in order to remove the copper catalyst. The organic layer was dried over anhydrous Na_2SO_4, filtered and concentrated under reduced pressure. The polymer was precipitated in MeOH, yielding a white solid which was dried under vacuum. δ_H ($CDCl_3$, 300 MHz) 7.36-6.38 (br. m, arom H), 4.48 (br. m, CH_2-C*H*(Ph)-Br), 2.17-1.24 (br. m, backbone CH_2, CH, ^{t}Bu), 0.98-0.84 (br. m, CO-C(CH_3)$_2$-CH_2). ν_{max}(solid)/cm^{-1} 3023, 2920, 1942, 1877, 1804, 1720 ($\nu_{C=O}$), 1600, 1491, 1450, 754, 696, 593. Characterization by SEC is summarized in Table 1.

Table 1 SEC and MALDI-ToF MS characterization of precursor polymers **1-4** and biohybrid amphiphiles **7-11**

Compound		SEC (THF)		SEC (NMP)					
		M_n (Da)	PDI	$M_{n,app}$[a] (Da)	PDI	n	M[b] calcd	*m/z* found	Assigned[c]
1a	^{t}BuO$_2$C-PS$_{21}$-Br	2260	1.11	2380	1.20	21	2408	n.d.	—
1b	^{t}BuO$_2$C-PS$_{49}$-Br	5330	1.13	5254	1.11	49	5325	n.d.	—
2a	HO$_2$C-PS$_{21}$-Br	2290	1.12	2750	1.14	21	2352	2350	$[M + H]^+$
2b	HO$_2$C-PS$_{49}$-Br	5350	1.14	6610	1.11	49	5269	n.d.	—
3a	^{t}BuO$_2$C-PS$_{21}$-N$_3$	2380	1.10	2710	1.13	21	2371	2393	$[M + Na]^+$
3b	^{t}BuO$_2$C-PS$_{49}$-N$_3$	5460	1.12	6330	1.10	49	5288	5310	$[M + Na]^+$
4	HO$_2$C-PS$_{21}$-N$_3$	2540	1.10	3020	1.15	21	2315	2338	$[M + Na]^+$
7a	Pept-PS$_{21}$-Br	—	—	5060	1.14	21	2780	2805	$[M + Na]^+$
7b	Pept-PS$_{49}$-Br	—	—	8090	1.05	49	5696	5721	$[M + Na]^+$
8	Pept-PS$_{21}$-N$_3$	—	—	7050	1.06	21	2744	2744	$[M + H]^+$
9a	^{t}BuO$_2$C-PS$_{21}$-Pept	—	—	6720	1.07	21	2914	2933	$[M + Na]^+$
9b	^{t}BuO$_2$C-PS$_{49}$-Pept	—	—	10970	1.09	49	5829	5828	$[M + H]^+$
10	HO$_2$C-PS$_{21}$-Pept	—	—	4345	1.56	21	2858	2856	$[M + H]^+$
11	Pept-PS$_{21}$-Pept	—	—	—[d]	—	21	3285	3282	$[M + H]^+$

[a] For the peptide-polymer conjugates an apparent Mn is reported based on a PS calibration set. [b] Calculated for the 100% isotope peak of M with the given number of repeating units (n). [c] The ion to which the found *m/z* value was assigned, with an error <0.01%. [d] An exceptionally broad peak was observed at high molecular weight, indicating the presence of aggregates. n.d. = not determined.

Polymer **1a** was prepared following a similar procedure with an adapted initiator/styrene ratio of 1 : 30.

α-Carboxylic acid-functionalized polystyrene (2, 4)

General procedure for the deprotection of the α-*tert*-butyl ester of PS: To a solution of α-*tert*-butylcarboxy PS in CH_2Cl_2 (typically 0.03 M) was added 50 equiv. of TFA. The mixture was stirred for 18 h at rt. Completion of the reaction was determined by TLC (CH_2Cl_2), which showed a dramatic decrease in R_f value upon deprotection. The mixture was washed with sat. $NaHCO_3$ (aq.) (2×) and the organic phase was dried over anhydrous Na_2SO_4, filtered and concentrated under reduced pressure. The residue was dissolved in CH_2Cl_2 and precipitated in MeOH. Filtration followed by drying *in vacuo* yielded the carboxylic acid terminated PS as a white powder. **2a**: quantitative yield, **2b**: 75%, **4**: 78%; ν_{max}(solid)/cm^{-1} **2a/b**: 3024, 2919, 1943, 1874, 1804, 1698 ($\nu_{C=O}$), 1600, 1492, 1451, 756, 696, 593; **4**: 3023, 2919, 2094 (ν_{N3}), 1938, 1869, 1800, 1700 ($\nu_{C=O}$), 1597, 1485, 1455, 759, 696, 538. Characterization by SEC and MALDI-ToF mass spectrometry is summarized in Table 1.

ω-Azido-functionalized polystyrene (3)

General procedure for substitution of the ω-bromide group of PS by an azide: To a solution of ω-bromo PS in anhydrous THF (typically 0.04 M) was added 8 equiv. of Me_3SiN_3 and 8 equiv. of TBAF (as a 1 M solution in THF) under a nitrogen atmosphere. After stirring for 18 h at rt, the mixture was concentrated under reduced pressure and precipitated in MeOH. The precipitate was filtered off and washed with MeOH thoroughly. The ω-azido terminated PS was obtained as a white solid which was dried *in vacuo*. **3a**: 90% yield, **3b**: 84%. δ_H (300 Mhz, $CDCl_3$) 7.36-6.38 (br. m, arom H), 3.95 (br. m, CH_2-C*H*(Ph)-N_3), 2.17-1.24 (br. m, backbone CH_2, CH), 0.97-0.84 (br. m, CO-C(CH_3)$_2$-CH_2. ν_{max}(solid)/cm^{-1} 3024, 2920, 2092, 1947, 1878, 1800, 1719, 1600, 1492, 1451, 756, 696, 538. Characterization by SEC and MALDI-ToF mass spectrometry is summarized in Table 1.

Peptide-PS conjugates *via* peptide coupling chemistry (7, 8)

Typical procedure (**7b**): A mixture of α-carboxylic acid PS **2b** (184 mg, 35.0 μmol), peptide **5** (40 mg, 77 μmol), *N*,*N*-diisopropyl ethylamine (DIPEA, 23 μL, 0.13 mmol), and DMF (15 mL) was cooled to 0 °C and stirred for 10 min. Subsequently, (benzotriazol-1-yl)oxytripyrrolidino-phosphonium hexafluorophosphate (pyBOP, 47 mg, 90 μmol) was added and the mixture was stirred for 30 min at 0 °C followed by 18 h at rt. Completion of the reaction was indicated by TLC analysis (CH_2Cl_2-MeOH, 9 : 1); **7b** slightly runs while the peptide (**5**) remains at the baseline and PS **2b** runs with the front. The reaction mixture was diluted with CH_2Cl_2 (20 mL) and washed with sat. $NaHCO_3$ (aq.) (20 mL). After concentrating the organic phase under reduced pressure, the mixture was purified by silica gel column chromatography (CH_2Cl_2-MeOH, 9 : 1), yielding **7b** as a white solid (137 mg, 72% yield). **7a**: 81%, **8**: 83%. Characterization by SEC and MALDI-ToF mass spectrometry is summarized in Table 1. Analysis by ^{1}H NMR spectroscopy was not performed since crucial signals indicative of covalent coupling between the peptide and polymer segments (*i.e.* amide or triazole protons) overlap with polystyrene signals.

Peptide-PS conjugates *via* the CuAAC (9, 10)

Typical procedure (**9a**): ω-azido PS **3a** (22 mg, 9.3 μmol) and peptide **6** (6 mg, 0.010 mmol) were dissolved in anhydrous DMF (5 mL) which was purged with nitrogen. The mixture was purged with nitrogen for another 10 min before a 1 : 1 complex of CuBr and tris(2-dimethylamino)ethyl)amine (Me_6TREN) was added as a 20 mM stock solution in nitrogen-purged DMF (1.0 mL, 0.020 mmol). The mixture was stirred at 40 °C for 48 h. Completion of the reaction was indicated by TLC analysis (CH_2Cl_2-MeOH, 9 : 1); **9a** slightly runs while the peptide (**6**) remains at the baseline and PS **3a** runs with the front. The reaction mixture was diluted with CH_2Cl_2 (10 mL) and washed with an aqueous solution of EDTA (10 mL, 0.065 M). After concentrating the organic phase under reduced pressure, the mixture was purified by silica gel column chromatography (CH_2Cl_2-MeOH, 9 : 1). Conjugate **9a** was obtained as a yellowish solid (18 mg, 64% yield). **9b**: 31%, **10**: 33%. Characterization by SEC and MALDI-ToF mass spectrometry is summarized in Table 1.

Synthesis of peptide-PS-peptide bolaamphiphile 11

A mixture of conjugate **10** (44 mg, 15 μmol), peptide **5** (12 mg, 23 μmol), *N*,*N*-diisopropylethylamine (DiPEA, 11 μL, 0.064 mmol), and DMF (3 mL) was cooled to 0 °C and stirred for 10 min. Subsequently, pyBOP (20 mg, 38 μmol) was added and the mixture was stirred for another 30 min at 0 °C followed by 18 h at rt. Completion of the reaction was indicated by TLC analysis (CH_2Cl_2-MeOH, 4 : 1), which showed an R_f value of ~0.35 for the product. After concentration under reduced pressure, the mixture was purified by means of preparative TLC (CH_2Cl_2-MeOH, 4 : 1). The desired product was extracted using a mixture of BuOH-AcOH-H_2O (16 : 4 : 1 v/v), resulting in a yellowish solid after concentration under reduced pressure (33 mg, 65% yield). Characterization by SEC and MALDI-ToF mass spectrometry is summarized in Table 1.

Results and discussion

Synthesis of PS-Gly-Gly-Arg-AMC amphiphiles

In order to use a single precursor polymer for the functionalization with a peptide by both the CuAAC and peptide coupling chemistry, we set out to prepare hetero-telechelic PS carrying a *tert*-butyl ester on one terminus and a bromide on the other end (**1**). Straightforward transformation of the *tert*-butyl ester into a carboxylic acid or the bromide functionality into an azide allows a peptide fragment to be coupled either through its free *N*-terminus or *via* an alkyne handle.

Precursor PS **1** was prepared by ATRP of styrene using *tert*-butyl-2-bromo-isobutyrate as an initiator with a CuBr/PMDETA catalyst in 10% anisole at 90 °C (Scheme 1). The polymer was synthesized with two average degrees of polymerization (DP), $n = 21$ (**1a**) and $n = 49$ (**1b**), both having a narrow molecular weight distribution (polydispersity index, PDI = 1.1, see Table 1) as determined by size-exclusion chromatography (SEC). Deprotection of the *tert*-butyl ester proceeded smoothly

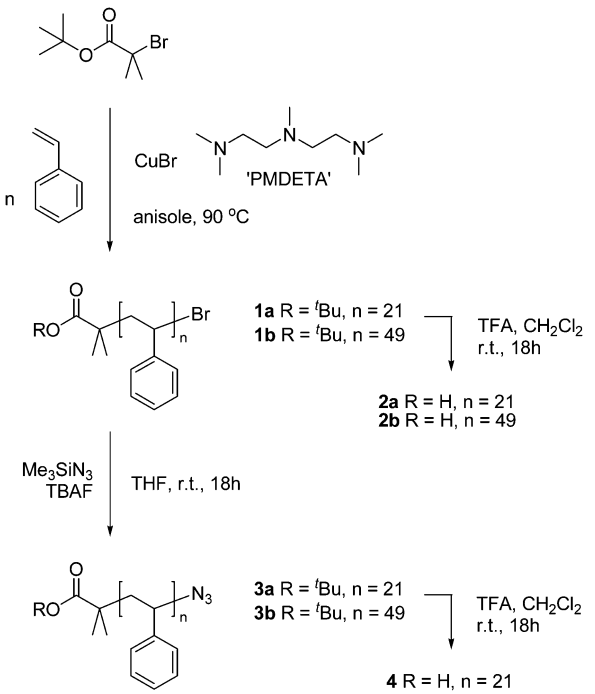

Scheme 1 Preparation of hetero-telechelic PS that is suitable for functionalization by peptide coupling chemistry and the CuAAC reaction.

with trifluoroacetic acid (TFA) and resulted in α-carboxylic acid-functionalized PS (**2**). Completion of the acid formation was determined by thin layer chromatography (TLC), which showed a dramatic decrease in R_f value (CH_2Cl_2 as the eluent) upon deprotection. Furthermore, a clear shift of the carbonyl stretch signal was observed by FTIR spectroscopy ($\nu_{C=O} = 1720\ cm^{-1}$ to $\nu_{C=O} = 1698\ cm^{-1}$).

The bromide end group of PS **1** was easily replaced by an azide *via* reaction with Me_3SiN_3 and TBAF in THF.[42,43] Complete conversion was confirmed by ^1H NMR spectroscopy, clearly showing a shift from $\delta = 4.41$ ppm to $\delta = 3.95$ ppm for the hydrogen neighboring the ω-end group. Additionally, analysis by FTIR spectroscopy showed the characteristic signal of an azide at 2092 cm^{-1} for the purified polymer. The ω-azido PS **3** can directly be used to couple alkyne-functionalized peptides. In addition, the α-*tert*-butyl ester of PS **3** can also be deprotected to yield α-carboxy ω-azido PS **4** which is ready for functionalization on both ends. Using the same conditions as for PS **1**, deprotection of PS **3** was readily achieved by treatment with TFA.

Having access to a set of polymer building blocks (**1-4**), we explored the modular synthesis of peptide-polymer amphiphiles as outlined in Scheme 2. As the peptide part, H-GlyGlyArg-AMC (**5**) and its corresponding alkyne-derivative **6** were employed (see ESI† for synthetic details). We first focused on the CuAAC between azide-terminated PS (**3a/b**) and peptide **6** in a similar way to that we have reported previously.[11] To ensure complete solubility of all reaction partners, the coupling was carried out in DMF as a solvent. A strong complex of CuBr and tris(2-dimethylamino)ethyl)amine (Me_6TREN) was used as a catalyst because previous results suggested that coordination of copper to the arginine residue might hamper the coupling reaction. After stirring for 48 h at 40 °C under an inert atmosphere, TLC analysis indicated completion of the reaction. To remove the copper catalyst, the reaction mixture was washed with an aqueous solution of ethylenediaminetetraacetic acid (EDTA) before further purification by silica gel chromatography was applied.[44] The peptide-polymer hybrids were isolated in moderate yields (64% and 31% for **9a** and **9b**, respectively), which is comparable to earlier results.[11] Characterization of the biohybrids was carried out by SEC and matrix-assisted laser desorption/ionization - time of flight (MALDI-ToF) mass spectrometry. SEC was initially carried out with THF as the eluent but this resulted in a shift toward lower molecular weight going from the PS to the peptide-polymer hybrid. Changing the eluent to *N*-methylpyrrolidone (NMP), however, resulted in a clear shift to higher molecular weight (The SEC traces of **3a** and **9a** are depicted in Fig. 1), though the mass difference was larger than expected based on a PS calibration set. The different behavior of the biohybrids compared to PS is likely due to a change in hydrodynamic volume and different types of interactions with the column material.[45] As a result, only an apparent molecular weight of the biohybrids could be determined by SEC, and these values are reported in Table 1. Nonetheless, SEC clearly showed that a new product was obtained and additional UV detection at $\lambda = 330$ nm revealed the presence of the AMC moiety, thereby confirming the coupling of peptide **6** (Fig. 1). Further characterization by MALDI-ToF mass spectrometry showed a single molecular weight distribution which was in good agreement with the expected mass of the PS-peptide conjugate (Fig. 2 displays the MALDI-ToF mass spectra of **3a** and **9a**). An overview of all characterization data is presented in Table 1.

Next, the coupling between carboxylic acid-functionalized PS **2a/b** and H-Gly-Gly-Arg-AMC (**5**) was investigated. With the help of (benzotriazol-1-yl)oxytripyrrolidinophosphonium hexafluorophosphate (pyBOP) as a coupling reagent in DMF, the reaction was found to be completed within 18 h. Purification by silica gel column chromatography resulted in peptide-polymer hybrids **7a** and **7b** in reasonable to good yields (81% and 72%, respectively). The coupling of **4** and **5** was also carried out and gave rise to **8** in a comparable yield (83%). As for the biohybrids obtained *via* the CuAAC, the formation of the coupled products was confirmed by SEC and MALDI-ToF mass spectrometry (Table 1).

With two convenient coupling strategies at hand, we explored the synthesis of a biohybrid bolaamphiphile by sequential functionalization of α-carboxy ω-azido PS **4** with peptides **5** and **6**. As the introduction of a second peptide might complicate the work-up, it was decided to first carry out the coupling reaction giving the lowest isolated yield, *i.e.* the CuAAC reaction. Under the same conditions as mentioned above, PS **4** and peptide **6** were coupled together giving compound **10** in an isolated yield of 33% (see Table 1 for analytical details). Subsequent coupling with peptide **5** proceeded smoothly using pyBOP and the desired bolaamphiphile was obtained (65%) after purification by preparative TLC. MALDI-ToF mass spectrometry showed a clear shift in molecular weight distribution which was in good agreement with the expected mass (Fig. 3, Table 1).

Assembly behavior in aqueous media

As described above, a series of peptide-PS amphiphiles was at hand, including a novel peptide-based bolaamphiphile. The

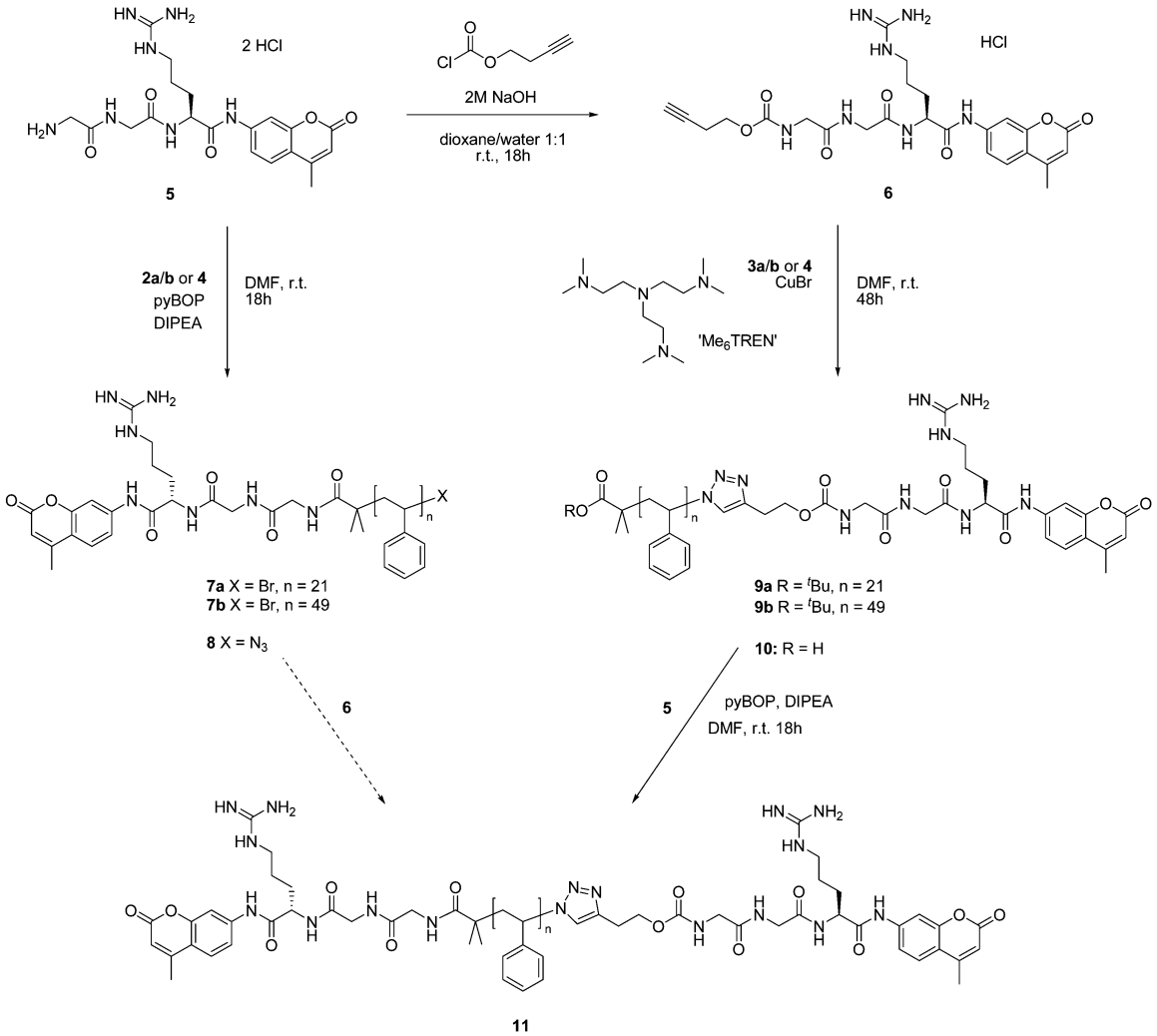

Scheme 2 Synthesis of biohybrid amphiphiles based on a PS tail and a Gly-Gly-Arg-AMC head group.

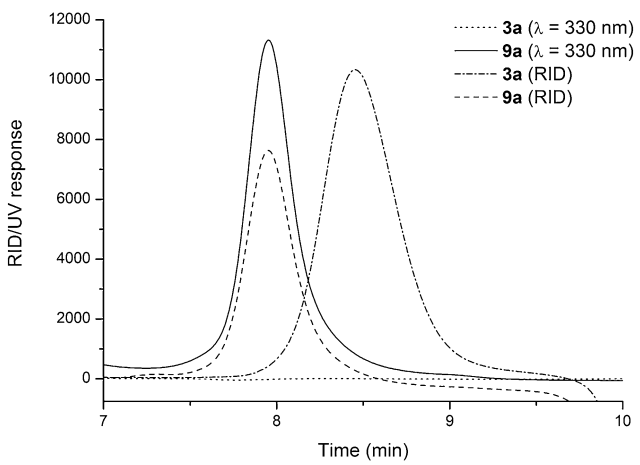

Fig. 1 SEC (NMP) trace of $^{t}BuO_2C$-PS_{21}-N_3 (**3a**) and $^{t}BuO_2C$-PS_{21}-Pept (**9a**) using RID and UV ($\lambda = 330$ nm) detection.

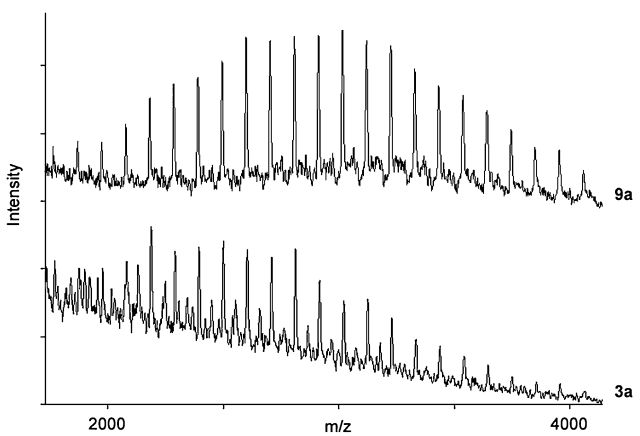

Fig. 2 MALDI-ToF mass spectra of $^{t}BuO_2C$-PS_{21}-N_3 (**3a**) and $^{t}BuO_2C$-PS_{21}-Pept (**9a**).

aggregation behavior of these biohybrid amphiphiles was examined in solution and at the air-water interface, as will be described below.

To induce self-assembly of peptide-polymer hybrids **7-10**, two procedures were employed: (i) injecting a THF solution of the biohybrids into water (to a final THF content of 9% v/v), and (ii) dialyzing the biohybrids against water starting from a solution in

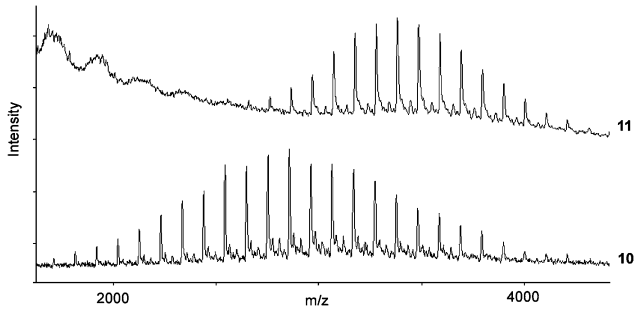

Fig. 3 MALDI-ToF mass spectra of HO_2C-PS_{21}-Pept (**10**), and Pept-PS_{21}-Pept (**11**).

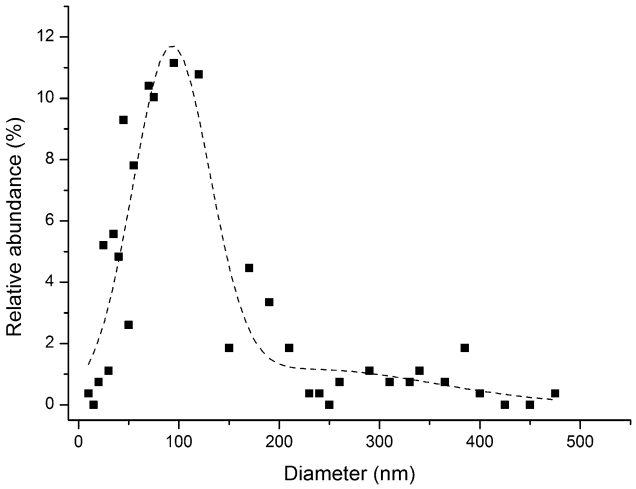

Fig. 5 Size distribution of assemblies formed by Pept-PS_{21}-Br (**7a**), as determined from multiple TEM-images (comprising Fig. 4A). The trendline is constructed from a Gaussian fit.

THF. Both methods resulted in cloudy mixtures, and transmission electron microscopy (TEM) revealed the formation of spherical aggregates with a rather large size distribution (30-500 nm) (Fig. 4). For biohybrid **7a**, a histogram of the aggregate sizes was constructed by measuring the size of structures (270 in total) from multiple TEM images (Fig. 5). The average diameter of the aggregates was determined to be 95 nm and the smallest structures of the population had a diameter of approximately 25-30 nm. The latter roughly corresponds to the expected length of four amphiphiles (see Fig. 6 for a basic model), which suggests that the assemblies were vesicular in nature. This is further supported by the fact that some of the larger assemblies contained a hole revealing a hollow interior (indicated by the arrows in Fig. 4). These holes were found to be most pronounced when aggregates were prepared by the injection method at 50 °C (Fig. 4D and ESI†). Besides the holes, it was noted that other defects such as disrupted membranes were present for some of the larger aggregates of biohybrid **8** (Fig. 4C).

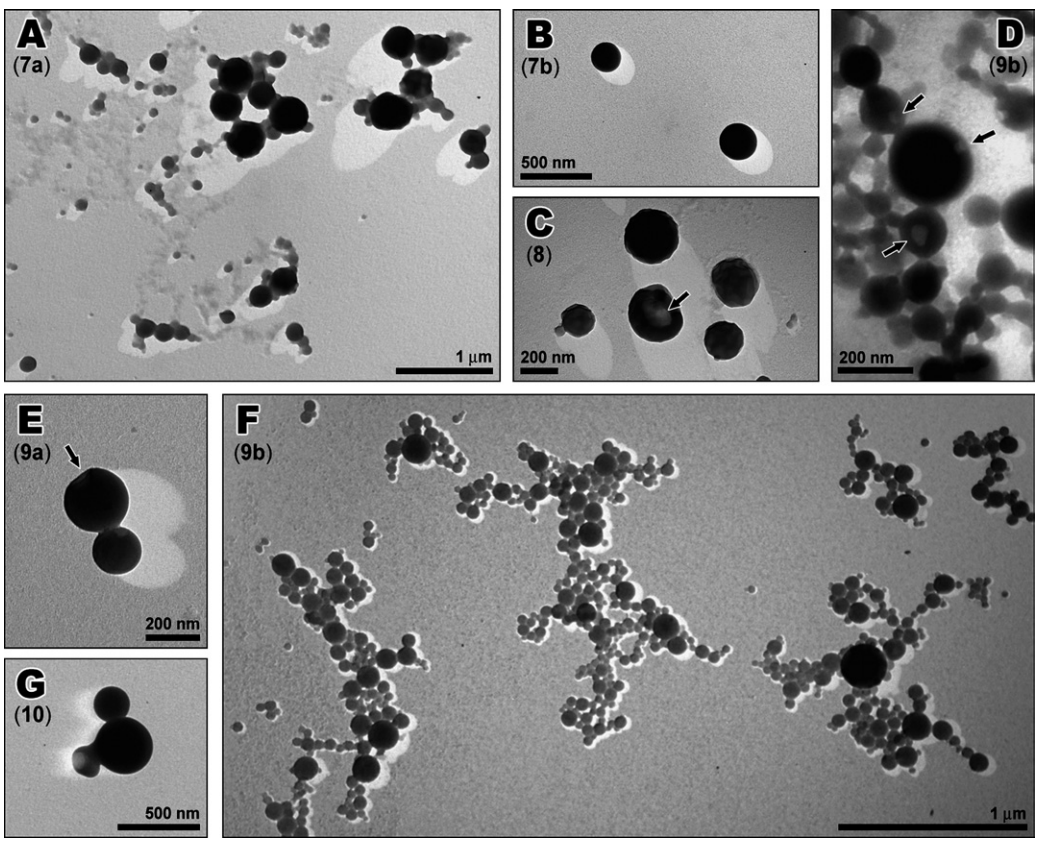

Fig. 4 TEM images of assemblies formed by peptide-PS amphiphiles **7-10**, Pt-shadowed except D. It should be noted that the shadow area may differ between images, not only due to the height of the assemblies but also because not all samples were prepared at the same time, leading to differences in the shadowing angle.

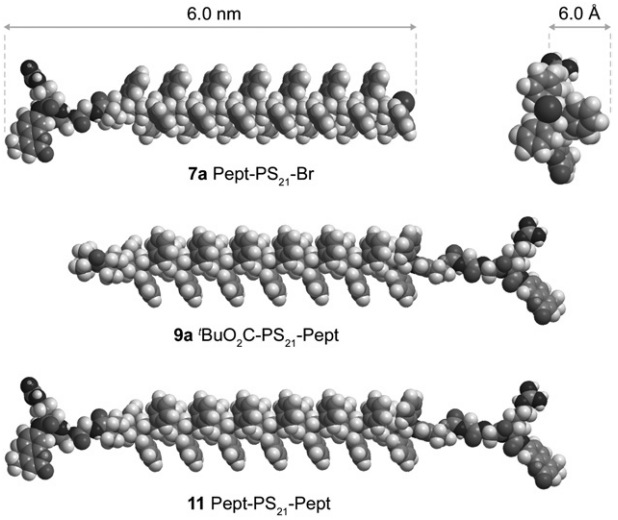

Fig. 6 Side-view and top-view of computer generated models of biohybrids **7a**, **9a**, and **11**.

Considering the cylindrical shape of the peptide-PS amphiphiles (Fig. 6), the formation of vesicles is in line with the concept of the molecular packing parameter.[46] This concept was established for phospholipids and associates the self-assembly behavior of an amphiphile with its shape being defined in terms of a packing parameter; $P = v/al$, where v is the volume of the tail, l is the length of the tail and a is the equilibrium area per molecule at the aggregate surface. For cylindrically-shaped amphiphiles P ranges from 0.5 to 1 and these compounds typically form vesicular assemblies. It should be noted that more advanced theory is available for the description of the self-assembly behavior of block copolymers,[47] however, given the structural analogy between our relatively small peptide-PS hybrids and traditional amphiphiles (*e.g.* phospholipids), the classical concept of molecular packing parameter will be applied. Following the definition of P, the assembly behavior of a peptide-PS amphiphile is not expected to change upon varying the polymer length, because the volume-to-length ratio (v/l) of the tail would be unchanged and accordingly the packing parameter remains constant for a given head group.[48] Indeed, no clear differences could be observed when comparing various TEM images of peptide-PS amphiphiles with different polymer lengths (**7a** *versus* **7b**, and **9a** *versus* **9b**, with $P \approx 1$). The same holds for biohybrids with different end groups opposite to the peptide (**7a** *versus* **8**, and **9a** *versus* **10**).

The aggregate populations of biohybrids **7-10** were further studied by dynamic light scattering (DLS). Samples were prepared *via* dialysis and the average hydrodynamic radius (R_H) of the aggregates was determined by CONTIN analysis[49] at scattering angles of 30° and 60° (Table 2). The peak width at half height was determined as a measure for the polydispersity of the assemblies (Table 2, presented in brackets). For almost all samples the average hydrodynamic radius was dependent on the scattering angle, which can be attributed to the rather broad size distribution of the aggregate population (illustrated by the peak width at half height and the observations by TEM). The angular dependency was less pronounced for biohybrids **9b** and **10**, which could perhaps be explained by the presence of a relatively high number of large aggregates that overshadowed the scattering contribution of the population's smaller share.[50] The fact that the scattering signal of a disperse mixture is dominated by its largest particles may also be the reason why the average hydrodynamic radii determined by DLS were drastically larger than the sizes found by TEM measurements.

Table 2 Hydrodynamic radii of assemblies formed by biohybrids **7-11** in water, determined by CONTIN analysis of DLS measurements at different scattering angles

Compound		R_H at 30°/nm	R_H at 60°/nm
7a	Pept-PS_{21}-Br	170 (116)[a]	130 (167)
7a[b]	Pept-PS_{21}-Br	200 (151)	98 (110)
7b	Pept-PS_{49}-Br	151 (184)	123 (65)
8	Pept-PS_{21}-N_3	190 (140)	93 (50)
9a	$^tBuO_2C$-PS_{21}-Pept	170 (109)	127 (82)
9b	$^tBuO_2C$-PS_{49}-Pept	348 (263)	323 (106)
10	HOOC-PS_{21}-Pept	215 (170)	214 (267)
11[c]	Pept-PS_{21}-Pept	259 (180)	192 (142)

[a] Peak width at half height. [b] Duplicate using the same sample preparation. [c] Dialyzed from DMF instead of THF.

Similar to the analysis by TEM, the particle sizes determined by DLS (Table 2) showed no clear trends with respect to variations in the chemical structure of the amphiphiles (*i.e.* PS length and end group composition). It should be noted that preparing two samples from the same batch of Pept-PS_{21}-Br (**7a**) resulted in a substantial difference in the average radius (entries 1 and 2, Table 2), thus changes in the DLS data should be interpreted with great care.

The self-assembly behavior of bolaamphiphile **11** was studied in a similar way as for the regular amphiphiles, though the biohybrid was dialyzed against water from a solution in DMF because it was poorly soluble in THF. After dialysis, a cloudy mixture was obtained and DLS measurements indicated the presence of assemblies with a radius somewhat larger than most of the regular PS-peptide amphiphiles (Table 2).[51] Attempts to prepare samples for TEM using the same method as for the regular amphiphiles (*i.e.* placing a carbon-coated copper grid on top of a sample droplet followed by the removal of the excess water with paper) were unsuccessful and showed no structures. However, drop-casting an aggregate sample of **11** onto a grid followed by drying in air gave rise to TEM images as displayed in Fig. 7A. The observed structures seemed to comprise a network of collapsed spherical assemblies, of which some substructures appeared to be hollow inside (indicated by the arrows in Fig. 7A). This suggests that biohybrid bolaamphiphile **11** may also form vesicular assemblies. Such vesicles could either be build-up from a monolayer membrane or a bilayer membrane consisting of two opposing hairpin-like molecules. The latter is perhaps rather unlikely because the PS chain is relatively short (DP = 21) and folding back appears unfavorable.

To acquire a more accurate view of the assemblies present in solution, cryo-scanning electron microscopy (cryo-SEM) studies were performed (Fig. 7B). In this case only separated assemblies were observed which had a spherical or ellipsoidal shape. The diameters of the assemblies ranged from 30-300 nm with an average around 160 nm. In addition to spherical assemblies, also rod-like architectures were occasionally observed, having a diameter of approximately 190 nm (insert Fig. 7B).

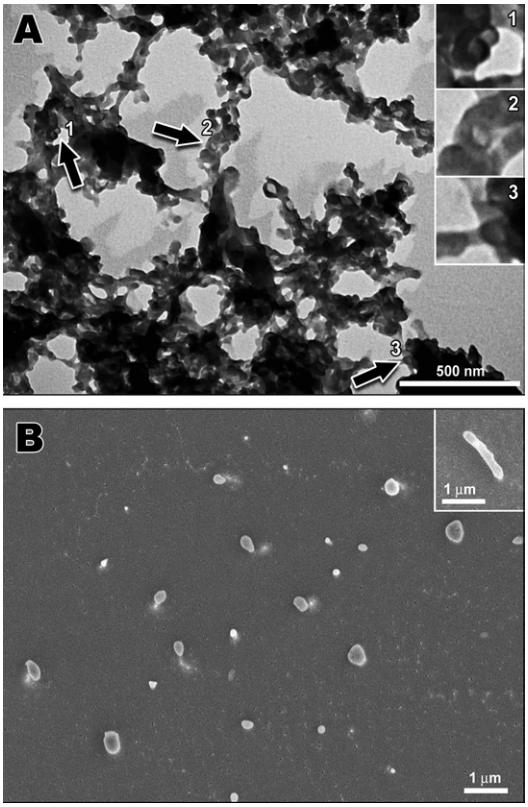

Fig. 7 TEM (A) and cyro-SEM (B) images of assemblies prepared from Pept-PS_{21}-Pept **11** by dialysis against water from a DMF solution. The arrows and numbers in the TEM image indicate the 3-fold magnification areas depicted on the upper right.

Assembly behavior at the air-water interface

In aqueous solution, the series of peptide-PS amphiphiles (**7-10**) self-assembled into vesicles. As expected based on the small changes in the molecular packing parameter, structural variations in the tail of the amphiphile did not affect the general self-assembly behavior of the compounds in water. However, to further examine the influences of structural differences on the packing of the amphiphiles, we studied the assembly behavior of biohybrids **7-10** at the air-water interface. Furthermore, monolayer investigations may clear up the problem of the orientation of bolaamphiphile **11** in the 3D assemblies discussed above.

Monolayers were prepared by spreading a chloroform solution of peptide-PS amphiphiles **7-10** on a water surface. To dissolve bolaamphiphile **11**, 5% of MeOH was added to the chloroform, or alternatively a dilute solution in 1,2-dichloroethane (DCE) was used to prepare the monolayer. Compression of the monolayers resulted in the pressure-area (Π-A) isotherms depicted in Fig. 8 and 10-12. All isotherms were recorded at least in duplicate and proved to be reproducible.

First, the isotherm of Pept-PS_{21}-Br (**7a**) will be discussed. In this isotherm four distinct phases were found, indicated by the numbers 1-4 in Fig. 8. A schematic representation of the amphiphile's arrangement in the four-phase regions is proposed in Fig. 9. At large surface area (phase 1) the peptide part is adsorbed at the air-water interface and the PS chain points away from the surface. The polymer will presumably be slightly coiled instead of being completely stretched-out perpendicular to the surface. In this first stage the molecules are not in contact with each other (constant surface pressure), hence, it can be considered as a *gaseous* phase. Upon compression of the monolayer a phase transition was observed at a lift-off area of 162 $Å^2$/molecule. The surface pressure increased rapidly and at 25 mN m^{-1} (phase 2) the monolayer was transferred to a carbon-coated copper grid. Subsequent TEM analysis showed that a homogenous film was formed (Fig. 8), indicating that the amphiphiles come in contact with each other and get packed fairly densely. Nonetheless, the monolayer could reversibly be compressed and decompressed (Fig. 14, discussed below) and the state can be considered a *liquid* phase. In the transition from the *gaseous* to

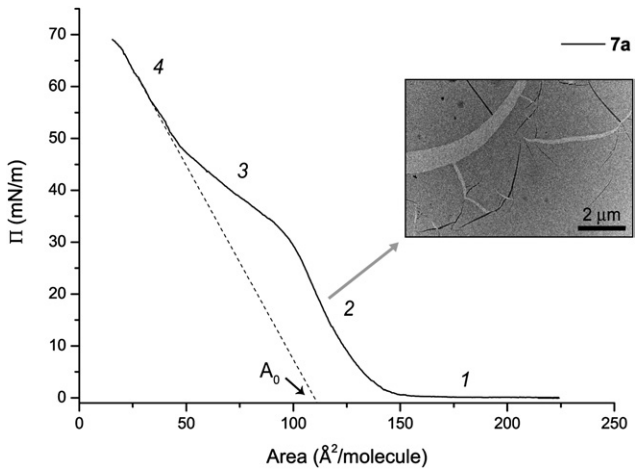

Fig. 8 Compression Π-A isotherm of Pept-PS_{21}-Br (**7a**) at 22 °C, and TEM image of the film lifted from the surface in phase 2.

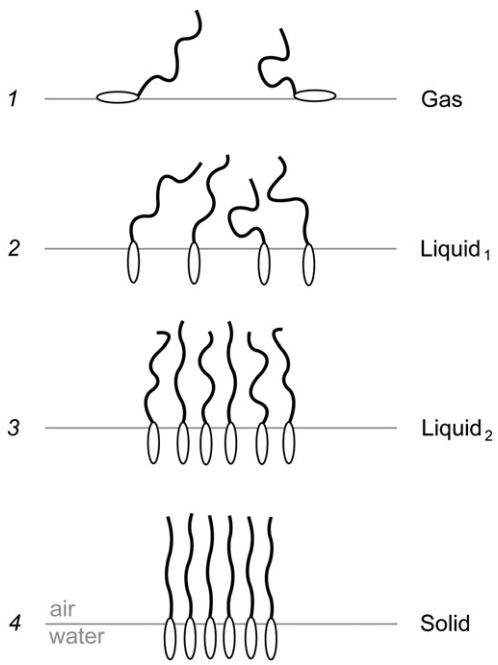

Fig. 9 Schematic representation of the phases in a monolayer of Pept-PS_{21}-Br (**7a**).

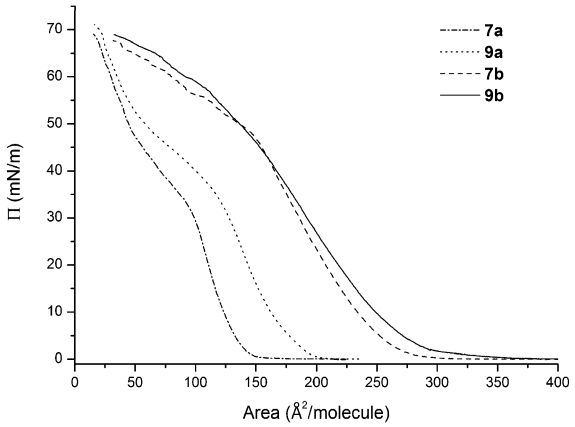

Fig. 10 Interfacial Π-A isotherms of peptide-PS amphiphiles with similar structures but different PS length; Pept-$PS_{21/49}$-Br (**7a/b**) and $^{t}BuO_2C$-$PS_{21/49}$-Pept (**9a/b**), at 22 °C.

liquid phase, the peptide segments are probable forced into the subphase at first contact of the molecules. Then, the polymer chains get packed together leading to a rapid increase in surface pressure. Around a surface pressure of 30 mN m^{-1} the slope of the isotherm leveled off (phase 3), indicating that the polymers reorganized to gain more space. Presumably here the PS chains undergo a transition from slightly coiled to stretched-out. This stage we also considered to be liquid-like and therefore phases 2 and 3 have been labeled as *liquid*$_1$, and *liquid*$_2$, respectively. Further compression of the *liquid*$_2$ phase resulted in a steeper rise in surface pressure. At that point (phase 4), probably all polymer chains are stretched-out and get condensed; forming a *solid* state. Extrapolating the steepest part of the isotherm in the *solid* phase results in a zero area (A_0) of 110 Å^2/molecule. This value is in good agreement with the 113 Å^2/molecule estimated for the fully stretched cylindrical peptide-PS conjugate depicted in Fig. 6 (the radius of this cylinder is approximately 6 Å). At high surface pressures and low area, the monolayer finally collapsed and here PS chains slide over each other to form three-dimensional structures. As a result, the isotherm could not be decompressed reversibly after reaching the *solid* phase, but instead the surface pressure dropped and no well-behaved monolayer was reformed.

Next, the isotherms of peptide-PS hybrids with different polymer lengths and chain ends will be discussed based on the conformations depicted in Fig. 9. The Π-A isotherms of peptide-PS conjugates with a similar chemical structure but a different PS length are depicted in Fig. 10. Comparing **7a** to **7b** and **9a** to **9b**, the length of the PS proved to have a clear influence on the lift-off area (Table 3), suggesting that the first phase transition is dominated by steric interactions between the polymer chains. This matches with the conformations we proposed for the *gaseous* and *liquid*$_1$ phase, in which the polymer chains are slightly coiled and longer polymers will thus take up more space than their shorter equivalents. The isotherms of the amphiphiles with the longer PS block do not reach a clear *solid* phase, and perhaps these chains do not all get fully stretch before interchain interactions promote a partial collapse into multilayered structures. While the isotherms of biohybrids **7b** and **9b** are almost superposable, the curves of the corresponding smaller amphiphiles **7a** and **9a** showed a substantial difference in their lift-off area. This suggests that there is a contribution of the peptide head group in the transition from *gas* to *liquid*, supporting the postulation that the peptide part is initially adsorbed onto the surface. However, the difference in lift-off area is much greater than the difference in size of the hydrophilic peptide part, which indicates that the nature of the polymer-peptide linkage (*i.e.* amide or triazole) has an effect on the positioning of the PS chain. For the longer amphiphiles the contribution of head groups is largely overshadowed by the interactions among the polymer chains.

Comparing the isotherms of amphiphiles with the same PS and peptide part but different opposing end groups (**7a** *versus* **8**, and **9a** *versus* **10**) showed some remarkable differences in the lift-off areas (Fig. 11, Table 3). Assuming that the first phase transition (from *gas* to *liquid*) is dominated by interactions among the PS chains, the differences suggest that end groups play a serious role in these interactions. The more bulky and less polarized end groups showed the highest lift-off areas; Br *versus* N_3, and $^{t}BuO_2C$ *versus* HOOC. These bulky and less polarized groups may lead to more repulsive forces between the chain ends causing a rise in surface pressure at larger area. All isotherms showed a similar shape with a clear region ascribed to the *solid* phase. Extrapolating the steepest part of this region resulted in the A_0 values presented in Table 3. The variations in the zero pressure are smaller than in the lift-off area, and these values are all in the range of the estimated value of 113 Å^2/molecule. Only the carboxylic acid terminated biohybrid showed a slightly higher A_0

Table 3 Lift-off areas and A_0 values for biohybrids **7-11** determined from their interfacial Π-A isotherms

Compound		Lift-off area (Å^2/molecule)	A_0 (Å^2/molecule)
7a	Pept-PS_{21}-Br	155	110
7b	Pept-PS_{49}-Br	294	—
8	Pept-PS_{21}-N_3	129	106
9a	$^{t}BuO_2C$-PS_{21}-Pept	203	119
9b	$^{t}BuO_2C$-PS_{49}-Pept	302	—
10	HOOC-PS_{21}-Pept	193	129
11	Pept-PS_{21}-Pept	62	—

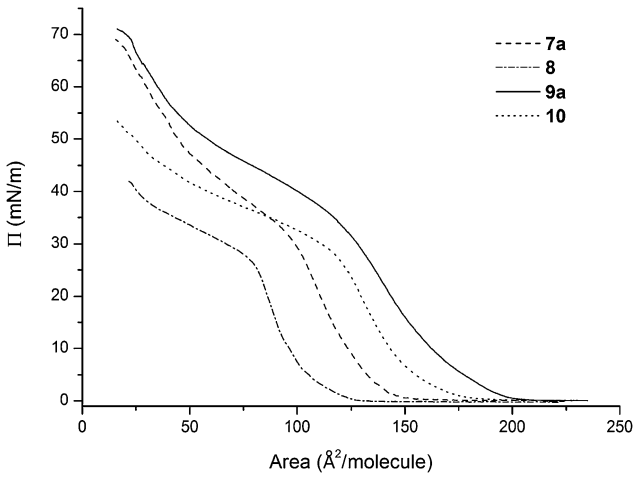

Fig. 11 Interfacial Π-A isotherms of peptide-PS amphiphiles with different end groups opposite to the peptide part; Pept-PS_{21}-Br/N_3 (**7a/8**) and $^{t}BuO_2C$/HOOC-PS_{21}-Pept (**9a/10**), at 22 °C.

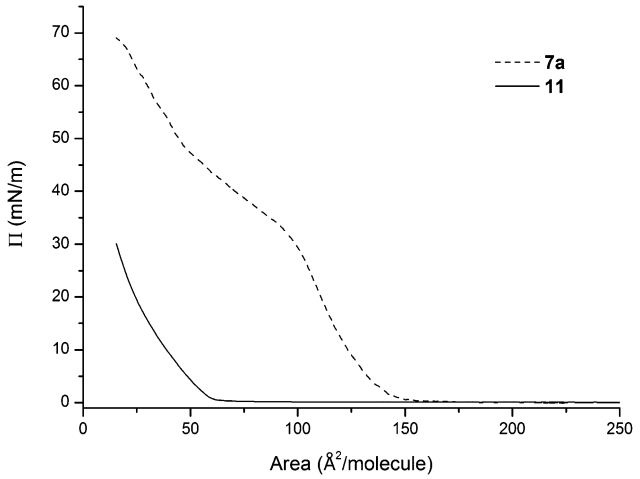

Fig. 12 Interfacial Π-A isotherms of Pept-PS_{21}-Br (**7a**) and Pept-PS_{21}-Pept (**11**) at 22 °C.

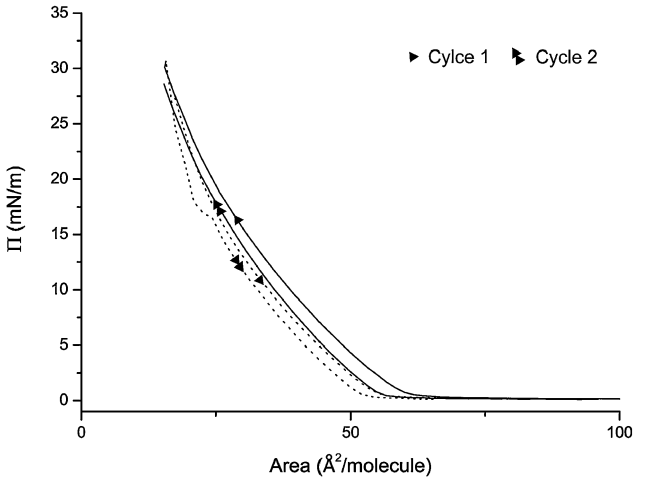

Fig. 13 Compression-decompression Π-A isotherms of Pept-PS_{21}-Pept (**11**) at 22 °C.

value (129 Å²/molecule), which might be explained by (hydrogen bonding) interactions between the chain ends affecting the conformation of the (stretched) PS chains.

The isotherm of bolaamphiphile **11** (Fig. 12) was strikingly different from those obtained for the other amphiphiles and showed a much smaller lift-off area (approximately 60 Å²/molecule), independently of the solvent from which the compound was spread on the surface. The fact that the lift-off area is much smaller than the estimated molecular diameter of a fully stretched amphiphile suggests that multilayered structures exist on the surface. A reason for the formation of these structures might be that the peptides on both sides of the polymer chain interact (*e.g. via* hydrogen bonding) in such a way that stabilized dimeric or multimeric architectures are formed.[52] However, no conclusive evidence for the arrangement of the amphiphiles was found by TEM analysis and initial AFM studies on the film of biohybrid **11** (data not shown).

At the endpoint of the compression isotherm (*i.e.* 30 mN/m and 20 Å²/molecule), the film of biohybrid **11** could reversibly be expanded, though the curve was not completely superposable with the preceding compression curve (Fig. 13). Upon a second compression, a smaller lift-off area was observed in comparison to the first isotherm, and expansion of the film again resulted in a curve which did not completely follow the preceding path. These hysteresis phenomena could imply that under compression some material is irreversible pushed into the subphase. However, it could also indicate that the amphiphiles only slowly reorganize within the film and insufficient time is allowed for the macromolecules to regain the gaseous conformation. Similar hysteresis effects as described above were also observed for biohybrid **7a** upon expanding of the monolayer from the *liquid*$_1$ phase (Fig. 14). For amphiphiles in this phase it is not likely that the hysteresis is caused by expelling material into the water, because this would only be favorable for bilayered structures. Therefore, the aforementioned kinetic parameters may play a role.

Unfortunately, the Π-A isotherm of bolaamphiphile **11** provided no hints as to whether the block copolymer packs in a stretched or folded conformation. Thus, the packing of **11** in its 3D assemblies formed in water remains unclear. Linking the monolayer studies of

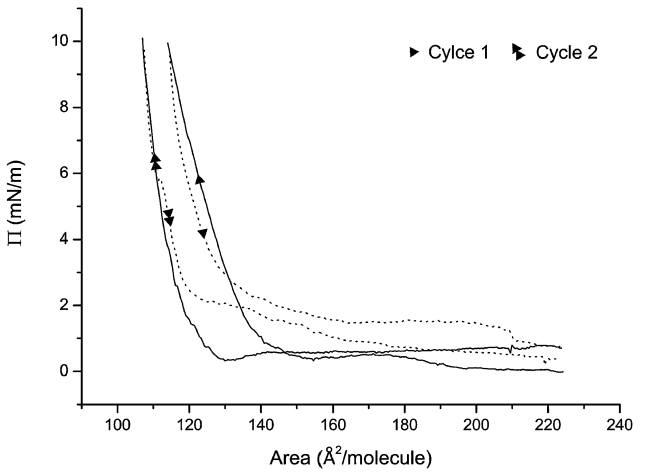

Fig. 14 Compression-decompression Π-A isotherms of Pept-PS_{21}-Br (**7a**) at 22 °C.

the regular amphiphiles (**7-10**) to their 3D assemblies, can probably be done best by considering the macromolecular ordering in the *solid* phase. This phase most likely resembles the situation of stretched amphiphiles as existing in a bilayer. As indicated by the A_0 values reported in Table 3, the lower molecular weight biohybrids (DP = 21) have comparable condensed phases, which matches the observation that similar assemblies were obtained in solution. Although at the air-water interface no clear *solid* phase was observed for the longer amphiphiles (**7b** and **9b**, DP = 49), these compounds will most probably also take up an extended conformation when present in a bilayer. Since all PS blocks have a molecular weight far below the entanglement molecular weight of PS ($M_e = 15.9 \pm 2.9$ kg mol^{-1}),[53,54] a stretched conformation is, in principle, possible for all amphiphiles studied.

Conclusions

In this report we have demonstrated that a small series of amphiphilic peptide-polystyrene block copolymers can be

prepared in a modular fashion *via* the CuAAC or peptide coupling chemistry. Both strategies proved to be efficient for the coupling of GlyGlyArg derivatives to PS, but the peptide coupling offered a more convenient protocol.

Using the same hetero-telechelic PS (DP = 21 or 49) as a precursor for both conjugation strategies, a series of peptide-polymer hybrid amphiphiles was prepared having small structural variations. Sequential employment of the two coupling methods gave rise to an ABA-type triblock copolymer, which can be considered as a macromolecular bolaamphiphile. As the two coupling techniques are orthogonal, also asymmetric types of bolaamphiphiles are expected to be accessible *via* the reported synthetic strategy. The aggregation behavior of the biohybrid amphiphiles and bolaamphiphile was investigated in solution and at the air-water interface. In water, the series of regularly-shaped (*i.e.* AB-type) amphiphiles formed comparable vesicular aggregates, which is in line with the expectations based on their modeled structures and simple packing parameter considerations. The bolaamphiphile also formed spherical assemblies, but more research is needed to clear up its exact mode of self-assembly.

In the monolayer experiments of the regular amphiphiles, variations in PS length were found to significantly affect the first phase transition (DP = 49 giving higher lift-off areas compared to DP = 21). This indicates that steric interactions among the chains play an important role in the transition, demonstrating that the polymers initially are somewhat coiled instead of being completely stretched out perpendicular to the surface. In addition to the polymer length, also the types of end groups opposite to the peptide were shown to have an effect on the first phase transition (comparing biohybrids with DP = 21). This effect was unexpectedly large, and further studies are required to completely get more insight in this phenomenon. Upon reaching a final condensed phase, the effect of the end groups greatly diminished and comparable extrapolated zero pressures were found. At this condensed phase the polymers are expected to be fully stretched, which resembles the orientation of amphiphiles in a bilayered vesicle. For the bolaamphiphile, unfortunately, the interfacial behavior could not be related to the behavior in solution, probably because multilayered structures existed on the water surface.

As peptide-polymer amphiphiles are promising compounds for the construction of bioactive nano-sized materials, finding appropriate synthetic methods and understanding their aggregation behavior is of general interest. Therefore, the synthetic strategies and self-assembly studies presented in this work are expected to be of relevance in exploring the chemistry of other peptide-polymer amphiphiles, leading to potential applications in *e.g.* diagnostics.

Acknowledgements

The authors would like to thank J. C. Gielen and Dr. P. C. M. Christianen for their help with the DLS measurements. The reported investigations were supported by the research school NRSC-Catalysis, the Chemical Council of the Netherlands Organization for Scientific Research (CW-NWO), the Netherlands Technology Foundation (STW) and the Royal Netherlands Academy of Arts and Sciences.

References and notes

1 R. S. Tu and M. Tirrell, *Adv. Drug Deliv. Rev.*, 2004, **56**, 1537–1563.
2 D. W. P. M. Löwik and J. C. M. van Hest, *Chem. Soc. Rev.*, 2004, **33**, 234–245.
3 Y.-Y. Luk and N. L. Abbott, *Curr. Opin. Colloid Interface Sci.*, 2002, **7**, 267–275.
4 (*a*) D. W. P. M. Löwik, J. Garcia-Hartjes, J. T. Meijer and J. C. M. van Hest, *Langmuir*, 2005, **21**, 524–526; (*b*) D. W. P. M. Löwik, I. O. Shklyarevskiy, L. Ruizendaal, P. C. M. Christianen, J. C. Maan and J. C. M. van Hest, *Adv. Mat.*, 2007, **19**, 1191–1195.
5 (*a*) J. D. Hartgerink, E. Beniash and S. I. Stupp, *Science*, 2001, **294**, 1684–1688; (*b*) J. D. Hartgerink, E. Beniash and S. I. Stupp, *Proc. Natl. Acad. Sci. USA*, 2002, **99**, 5133–5138.
6 G. A. Silva, C. Czeisler, K. L. Niece, E. Beniash, D. A. Harrington, J. A. Kessler and S. I. Stupp, *Science*, 2004, **303**, 1352–1355.
7 V. M. Yuwono and J. D. Hartgerink, *Langmuir*, 2007, **23**, 5033–5038.
8 Y.-B. Lim, E. Lee and M. Lee, *Angew. Chem. Int. Ed.*, 2007, **46**, 9011–9014.
9 L. Ayres, P. H. J. Adams, D. W. P. M. Löwik and J. C. M. van Hest, *J. Polym. Sci. Part A: Polym. Chem.*, 2005, **43**, 6355–6366.
10 M. L. Becker, J. Q. Liu and K. L. Wooley, *Biomacromolecules*, 2005, **6**, 220–228.
11 A. J. Dirks, S. S. van Berkel, N. S. Hatzakis, J. A. Opsteen, F. L. van Delft, J. J. L. M. Cornelissen, A. E. Rowan, J. C. M. van Hest, F. P. J. T. Rutjes and R. J. M. Nolte, *Chem. Commun.*, 2005, 4172–4174.
12 I. C. Reynhout, D. W. P. M. Löwik, J. C. M. van Hest, J. J. L. M. Cornelissen and R. J. M. Nolte, *Chem. Commun.*, 2005, 602–604.
13 (*a*) G. W. M. Vandermeulen, C. Tziatzios and H.-A. Klok, *Macromolecules*, 2003, **36**, 4107–4114; (*b*) G. W. M. Vandermeulen, C. Tziatzios, R. Duncan and H.-A. Klok, *Macromolecules*, 2005, **38**, 761–769; (*c*) I. W. Hamley, I. A. Ansari, V. Castelletto, H. Nuhn, A. Rösler and H.-A. Klok, *Biomacromolecules*, 2005, **6**, 1310–1315.
14 J. Nicolas, G. Mantovani and D. M. Haddleton, *Macromol. Rapid Commun.*, 2007, **28**, 1083–1111.
15 H. G. Börner, *Macromol. Chem. Phys.*, 2007, **208**, 124–130.
16 M. A. Gauthier and H.-A. Klok, *Chem. Commun.*, 2008, 2591–2611.
17 M. L. Becker, J. Q. Liu and K. L. Wooley, *Chem. Commun.*, 2003, 180–181.
18 Y. Mei, K. L. Beers, H. C. M. Byrd, D. L. Vanderhart and N. R. Washburn, *J. Am. Chem. Soc.*, 2004, **126**, 3472–3476.
19 R. M. Broyer, G. M. Quaker and H. D. Maynard, *J. Am. Chem. Soc.*, 2008, **130**, 1041–1047.
20 J. Couet, J. D. Jeyaprakash, S. Samuel, A. Kopyshev, S. Santer and M. Biesalski, *Angew. Chem. Int. Ed.*, 2005, **44**, 3297–3301.
21 J. Couet and M. Biesalski, *Macromolecules*, 2006, **39**, 7258–7268.
22 S. Loschonsky, J. Couet and M. Biesalski, *Macromol. Rapid Commun.*, 2008, **29**, 309–315.
23 H. Rettig, E. Krause and H. G. Börner, *Macromol. Rapid Commun.*, 2004, **25**, 1251–1256.
24 M. G. J. ten Cate, H. Rettig, K. Bernhardt and H. G. Börner, *Macromolecules*, 2005, **38**, 10643–10649.
25 M. G. J. ten Cate and H. G. Börner, *Macromol. Chem. Phys.*, 2007, **208**, 1437–1446.
26 J. Hentschel, M. G. J. ten Cate and H. G. Börner, *Macromolecules*, 2007, **40**, 9224–9232.
27 J. Hentschel, K. Bleek, O. Ernst, J.-F. Lutz and H. G. Börner, *Macromolecules*, 2008, **41**, 1073–1075.
28 K. Molawi and A. Studer, *Chem. Commun.*, 2007, 5173–5175.
29 C. J. Hawker, A. W. Bosman and E. Harth, *Chem. Rev.*, 2001, **101**, 3661–3688.
30 M. Kamigaito, T. Ando and M. Sawamoto, *Chem. Rev.*, 2001, **101**, 3689–3745.
31 K. Matyjaszewski and J. H. Xia, *Chem. Rev.*, 2001, **101**, 2921–2990.
32 V. V. Rostovtsev, L. G. Green, V. V. Fokin and K. B. Sharpless, *Angew. Chem. Int. Ed.*, 2002, **41**, 2596–2599.
33 C. W. Tornøe, C. Christensen and M. Meldal, *J. Org. Chem.*, 2002, **67**, 3057–3064.
34 V. D. Bock, H. Hiemstra and J. H. van Maarseveen, *Eur. J. Org. Chem.*, 2005, 51–68.
35 W. H. Binder and R. Sachsenhofer, *Macromol. Rapid Commun.*, 2007, **28**, 15–54.

36 J.-F. Lutz, *Angew Chem Int. Ed.*, 2007, **46**, 1018–1025.
37 A. J. Dirks, J. J. L. M. Cornelissen, F. L. van Delft, J. C. M. van Hest, R. J. M. Nolte, A. E. Rowan and F. P. J. T. Rutjes, *QSAR Comb. Sci.*, 2007, **26**, 1200–1210.
38 P. Wu, M. Malkoch, J. N. Hunt, R. Vestberg, E. Kaltgrad, M. G. Finn, V. V. Fokin, K. B. Sharpless and C. J. Hawker, *Chem. Commun.*, 2005, 5775–5777.
39 J.-F. Lutz, H. G. Börner and K. Weichenhan, *Macromolecules*, 2006, **39**, 6376–6383.
40 J.-F. Lutz, H. G. Börner and K. Weichenhan, *Aust. J. Chem.*, 2007, **60**, 410–413.
41 A. H. Fuhrhop and T. Y. Wang, *Chem. Rev.*, 2004, **104**, 2901–2937.
42 K. Matyjaszewski, Y. Nakagawa and S. G. Gaynor, *Macromol. Rapid Commun.*, 1997, **18**, 1057–1066.
43 J. A. Opsteen and J. C. M. van Hest, *Chem. Commun.*, 2005, 57–59.
44 After workup the copper content in a sample of biohybrid **9a** was determined to be less than 0.4 mol% (by atomic-absorption spectroscopy), demonstrating that the catalyst was effectively removed.
45 It should be noted that changing the polarity of the end group on PS also seriously affected the retention times in SEC using NMP as an eluent (Table 1).
46 (*a*) J. N. Israelachvili, D. J. Mitchell and B. W. Ninham, *J. Chem. Soc., Faraday Trans. II*, 1976, **72**, 1525–1568; (*b*) J. N. Israelachvili, S. Marcelja and R. G. Horn, *Quart. Rev. Biophys.*, 1980, **13**, 121–200.
47 M. Antonietti and S. Forster, *Adv. Mat.*, 2003, **15**, 1323–1333.
48 Assuming that the PS remains fully stretched, because upon folding the *v*/*l* ratio would obviously be changed. Moreover, only the effect on the general assembly behavior is considered here; so not the influence of polymer length on the thickness of the bilayer.
49 (*a*) S. W. Provencher, *Comput. Phys. Commun.*, 1982, **27**, 229–242; (*b*) S. W. Provencher, *Comput. Phys. Commun.*, 1982, **27**, 213–227.
50 The scattering intensity of a particle is proportional to the sixth power of its diameter according to Rayleigh's approximation.
51 Injecting the DMF solution of biohybrid **11** into water did not result in a cloudy mixture, thus the injection method was not further employed for the self-assembly studies.
52 It was noted that the fluorescence intensity of bolaamphiphile **11** in solution (under a standard UV lamp, $\lambda = 366$ nm) was lower than for a similar solution of biohybrids **7-10**, indicating that the coumarin moieties are in close proximity of each other, presumably leading to some quenching. Based on this observation, interactions among the bolaamphiphile could already exist before the sample was spread on the surface.
53 L. J. Fetters, D. J. Lohse and R. H. Colby, *Physical Properties of Polymers Handbook*, ed. J. E. Mark, American Institute of Physics: Woodburry, NY, 1996.
54 W. W. Graessley and J. Roovers, *Macromolecules*, 1979, **12**, 959–965.